Jour. Fac. Sci., Hokkaido Univ., Ser. VII (Geophysics), Vol. 10, No. 2, 269-293, 1997.

# Source Characteristics of the 1994 Hokkaido Toho-Oki Earthquake Deduced from Wide Band Strong Motion Records

**Tsutomu Sasatani**

*Division of Earth and Planetary Sciences, Graduate School of Science, Hokkaido University, Sapporo 060, Japan*

( Received December 4, 1996 )

**Abstract**

The Hokkaido Toho-Oki earthquake (MJMA 8.1), which occurred far east off Hokkaido, Japan, on October 4, 1994, has the following features: 1) the different mechanism from those of the large thrust earthquakes in this region; 2) an extremely large felt area; 3) anomalously large peak horizontal accelerations. On the other hand, the largest aftershock (MJMA 7.0) occurring on October 9, 1994, has the typical thrust event mechanism, and the felt area and the attenuation relation of peak accelerations are normal ones. These facts indicate the different source process between the main shock and the largest aftershock.

Wide band strong motion records during the 1994 Hokkaido Toho-Oki earthquake and its aftershocks were obtained at 4 sites ($\Delta=270\sim380$ km) located in the south-eastern part of Hokkaido. By comparing the wide band records from the main shock with those from the largest aftershock over the wide period range (0.05~100s), we extract unique source process of the main shock. First the displacement seismograms, in which long-period seismic waves predominate, are analyzed to study the total source process. The synthetic seismograms calculated for various source parameters are compared with the observed ones. We obtain the following results: (depth, $H$, source process time, $T$, seismic moment, $M_0$)=(~60 km, 30s, $2.9\times10^{21}$Nm) for the main shock and ($H$, $T$, $M_0$)=(~35 km, 15s, $8.5\times10^{19}$Nm) for the largest aftershock. Our results are nearly the same as those obtained by the other authors and indicate that the main shock is the lithospheric earthquake while the largest aftershock is the plate boundary earthquake. Second we analyze the vertical component velocity seismograms, in which intermediate-period seismic waves predominate, to extract more complex source process. In the P-wave portion from the main shock, several ripples with a period of several seconds appear about 10 seconds after the initial small, smooth phases (the rupture initiation phases). These ripples may correspond to seismic signals due to the complex source process such as the series of subevents. The distinct, source-effect ripples are not observed in the P-wave portion from the largest aftershock. Thirdly we study a short-period seismic wave radiation problem in the frequency domain. The transverse S-wave spectral ratios of the main shock to the largest aftershock are interpreted using the spectral ratio reference curves based on $\omega^{-2}$ source model and the source parameters obtained above. The interpretation indicates anomalously strong radiation of short-period (about 0.1s)

seismic waves during the main shock. Finally we examine the relation between the observed ripples and the short-period seismic wave radiation in the time domain. From a comparison of the vertical component accelerograms with the velocity seismograms in the P-wave portion, we find that the acceleration level grows up in proportion to the ripple amplitude during the main shock ; this indicates that the ripples and the strong radiation of short-period seismic waves have a cause-and-effect relationship. The wide band records during the 1993 Kushiro-Oki earthquake, a large lithospheric earthquake (MJMA 7.8), also show the same features as observed during the 1994 Hokkaido Toho-Oki earthquake.

## 1. Introduction

A large earthquake (MJMA 8.1) occurred far east off Hokkaido on October 4, 1994 (Fig. 1). This earthquake is named as the 1994 Hokkaido Toho-Oki earthquake by JMA (Japan Meteorological Agency). A large tsunami and strong shaking caused severe damage to the eastern part of Hokkaido and the southern part of the Kurile islands (e.g., Architectural Institute of Japan, 1996). This earthquake occurred at the similar source region of the 1969 Kurile Islands earthquake (MJMA 7.8) as shown in Fig. 1. Since the repeat time of large earthquakes along the Kurile islands is believed to be about 100 years (e.g., Utsu, 1972), the occurrence of this earthquake only 25 years after the 1969 event was initially considered somewhat unusual. However, several studies soon revealed that the 1994 earthquake is not a thrust event on the plate interface but an intra-plate event that ruptures through a substantial part of the subducting oceanic lithosphere (Kikuchi and Kanamori, 1995 ; Tanioka et al., 1995). The repeat time of large earthquakes in subduction zones is applied to large thrust earthquakes.

The 1994 Hokkaido Toho-Oki earthquake is characterized by an extremely large felt area. In Fig. 2, we compare distributions of seismic intensities (JMA scale) for the 1994 event and the 1969 event. In spite of nearly the same seismic moments for both events, the felt area for the 1994 event is much larger than that for the 1969 event. In addition to this, observed peak horizontal accelerations are extremely larger than those expected from the empirical attenuation relations as shown in Fig. 3. Unfortunately, we have no such data for the 1969 event. We take an interest in these characteristics and study wide band strong motion records during the 1994 Hokkaido Toho-Oki earthquake to understand reasons of them.

Kikuchi and Kanamori (1995) have studied the source process of the 1994 Hokkaido Toho-Oki earthquake using far-field body-waves (P and SH components) and long-period Love and Rayleigh waves. Their results are summa-

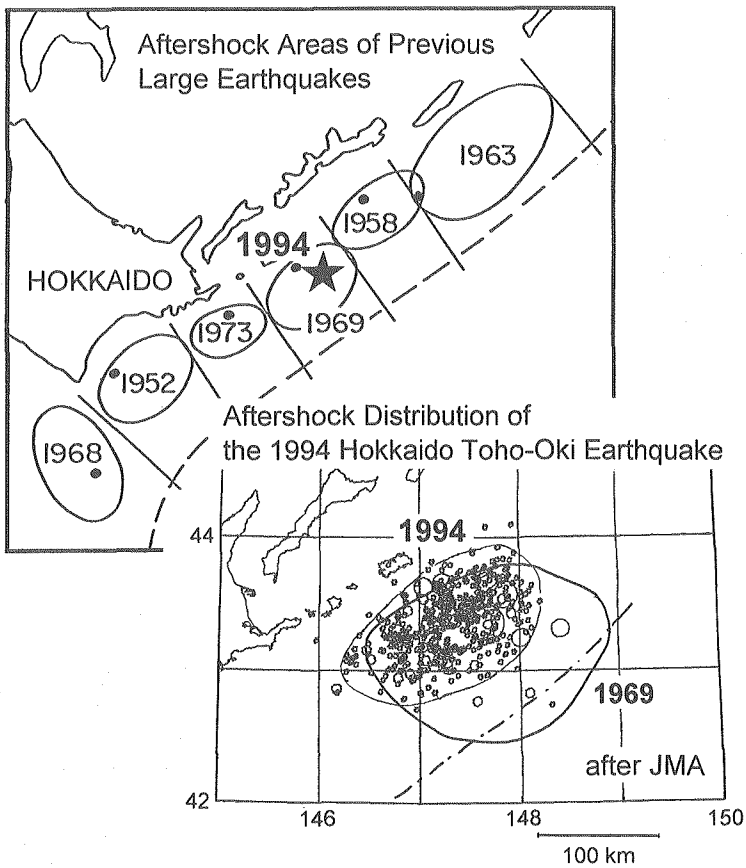


Fig. 1. Upper: Aftershock areas of previous large earthquakes in the Kurile Islands region. The epicenter of the 1994 Hokkaido Toho-Oki earthquake is shown by a star symbol. The base figure is taken from Fig. 12 of Fukao and Furumoto (1979). Lower: Aftershock distribution of the 1994 Hokkaido Toho-Oki earthquake after JMA. Also shown is aftershock area of the 1969 Kurile Islands earthquake by JMA.

rized as follows: 1) the mechanism is clearly different from those of the large earthquakes in this region that had occurred on the subduction plate boundary (see Fig. 2); 2) the large centroid depth (56 km) and the high stress drop (11 MPa) strongly suggest that the 1994 Hokkaido Toho-Oki earthquake is an intra-plate event or a lithospheric earthquake. Tanioka et al. (1995) also obtained nearly the same results. On the other hand, the largest aftershock ($M_{JMA}$ 7.0) occurring on October 9, 1994 has the typical thrust event mechanism

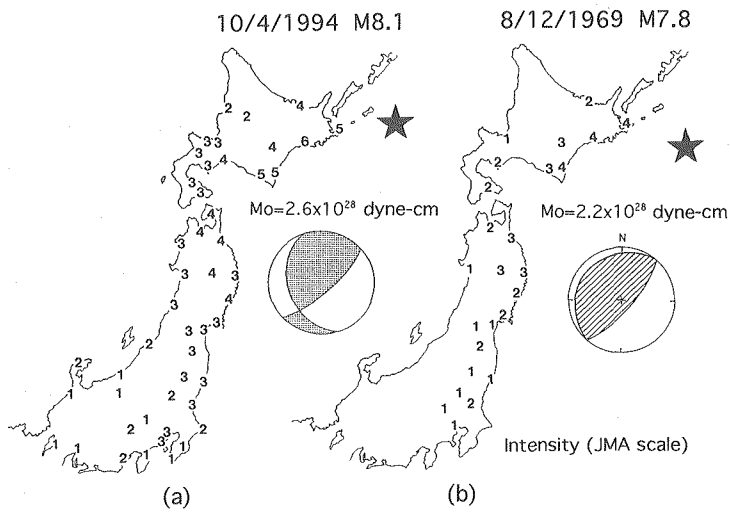


Fig. 2. Distribution of seismic intensities (JMA scale) in Japan for the 1994 Hokkaido Toho-Oki and the 1969 Kurile Islands earthquakes. Their focal mechanisms and seismic moments are also shown. These are taken from Kikuchi and Kanamori (1995) for the 1994 event and Abe (1973) for the 1969 event, respectively.

in this region (Dziewonski et al., 1995 ; see Fig. 4(a)). The felt area and the attenuation relation of peak accelerations for the largest aftershock are normal ones as shown in Fig. 4. These facts may indicate the different source process between the main shock and the largest aftershock.

Wide-band strong motions during the 1994 Hokkaido Toho-Oki earthquake and its aftershocks were observed at 4 sites located in the south-eastern part of Hokkaido. In this paper we analyze these records over the wide period range (0.05～100 s). By comparing the wide band strong motion records from the main shock with those from the largest aftershock, we will extract unique source process of the 1994 Hokkaido Toho-Oki earthquake. Hereafter we abbreviate the main shock and the largest aftershock to the 10/4 event and the 10/9 event, respectively.

## 2. Data

Strong motion data used in this study were obtained at 4 observation sites in Hokkaido as shown in Fig. 5. MYR is located on the rock site. OUV is located at the central part of the Tokachi plain which is the sedimentary basin covered mainly by terrace deposits. A thickness of the sedimentary layer

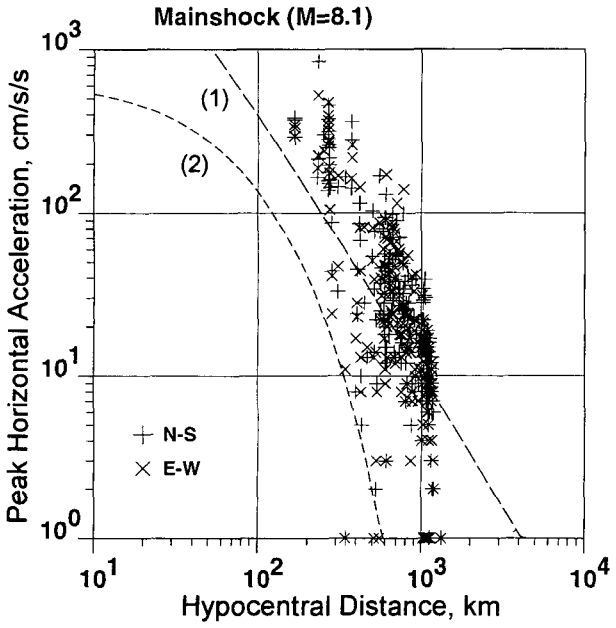


Fig. 3. Relationship between peak horizontal accelerations and hypocentral distances for the main shock. A curve (1) is the empirical attenuation relation by Kanai et al. (1966; $T_G=0.4$) which represents well the attenuation in the eastern part of Japan (Takemura, 1987), and a curve (2) is that by Fukushima and Tanaka (1990) which represents the average attenuation in Japan for shallow earthquakes.

beneath this site is about 600 m (Matsushima, 1990). TIS and KRK are located in Kushiro city and these belong to a part of the ESG Kushiro array (Fig. 5(b); Sasatani, 1996). TIS is on the lowland with an alluvial thickness of about 100 m, while KRK is on the hill zone. The boundary between the lowland and the hill zone is the Old Kushiro River. Wide frequency band, velocity-type strong motion seismometers (Muramatu, 1995) were installed at these stations; VS-1 (Tokyo Sokushin Co.) at TIS and VS-3 (Tokyo Sokushin Co.) at MYR, OUV and KRK. These have a wide flat response to ground velocity in the frequency range of 0.025 to 20 Hz (VS-1) and 0.002 to 30 Hz (VS-3) as shown in Fig. 6. The seismic signals were recorded by a digital recorder, PDAS-100 (Teledyne Co.) with a sampling frequency of 100 Hz and a resolution of 16 bit. These station informations are summarized in Table 1.

Figures 7 and 8 show observed velocity seismograms during the 10/4 and 10/9 events. Unfortunately, the horizontal components are off-scaled at KRK

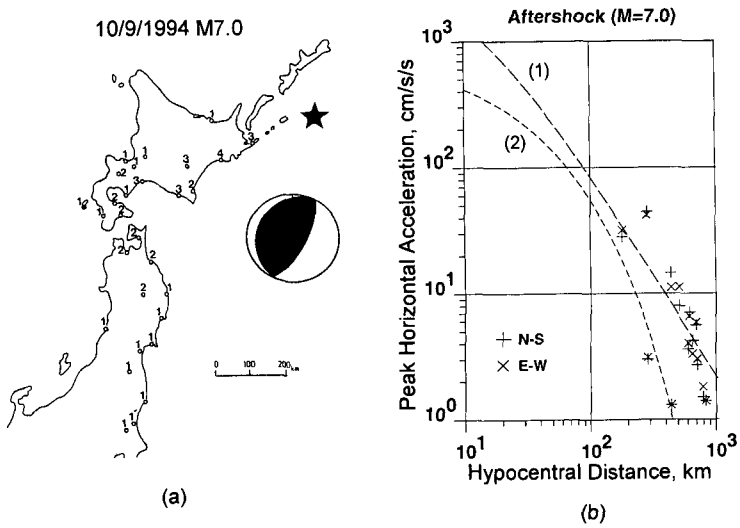


Fig. 4. (a) Distribution of seismic intensities (JMA scale) for the largest aftershock. Also shown is the focal mechanism by Dziewonski et al. (1995). (b) Relationship between peak horizontal accelerations and hypocentral distances for the largest aftershock. For curves (1) and (2), see the caption of Fig. 3.

during the 10/4 event. We use only the vertical component at this station in the following analysis. We can see different features among these seismograms depending on site conditions as mentioned above and event magnitudes. For example, the horizontal component seismograms at OUV have long duration later phases with a period of several seconds, which can be interpreted as the basin transduced surface waves (Furumura and Sasatani, 1996). The amplitudes of ground motions for the 10/4 event are about 10 times larger than those for the 10/9 event at each site. In the following sections, we analyze these records over the three period ranges; long-period seismic waves (10-100s), intermediate-period seismic waves (1-10s) and short-period seismic waves (0.05-1s). Our unique seismometers make it possible to analyze strong ground motions over the very wide period range.

## 3. Long-Period Seismic Waves

Here we analyze displacement seismograms obtained by integrating the velocity records. Figure 9 shows an example of the displacement seismograms from the 10/4 and 10/9 events at the rock site MYR. S pulse shape on the transverse component is relatively simple and the pulse width for the 10/4 events

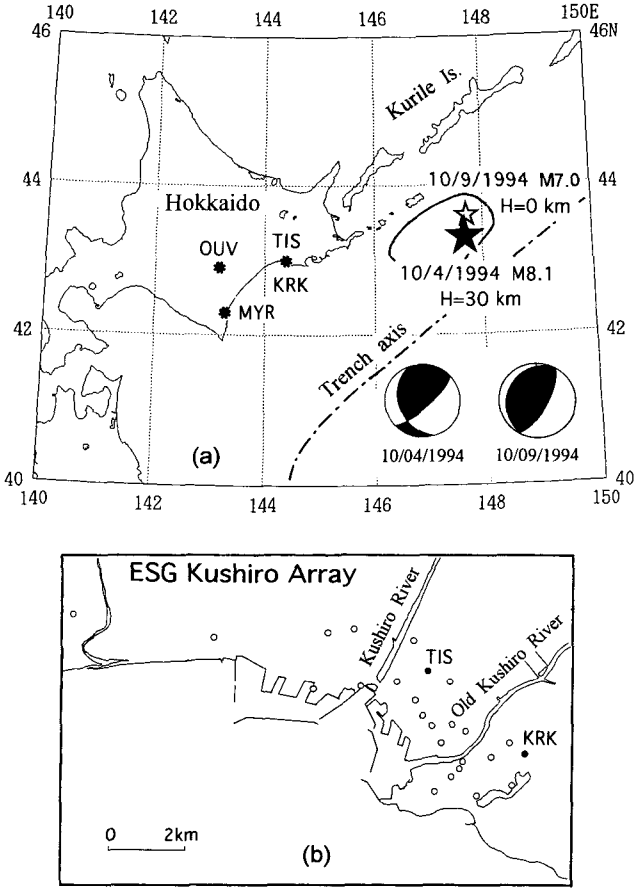


Fig. 5. (a) Location map showing epicenters of the main shock (★) and the largest aftershock (☆), and observation sites (●). The focal parameters are taken from JMA. (b) ESG cooperative strong motion observation sites in Kushiro city (Sasatani, 1996). Among these, TIS and KRK data are used in this study.

is much longer than that for the 10/9 event. Surface waves predominate in the seismograms for the 10/9 event. These features provide informations about the total source process.

Recently the detailed source process has been estimated by using the inversion method based on many strong motion records around the source region (e.g., Wald et al., 1996; Sekiguchi et al., 1996). However, our strong motion records are obtained relatively far from the source region and their azimuthal coverage is very narrow (Fig. 5(a)). Thus we cannot apply the inversion method

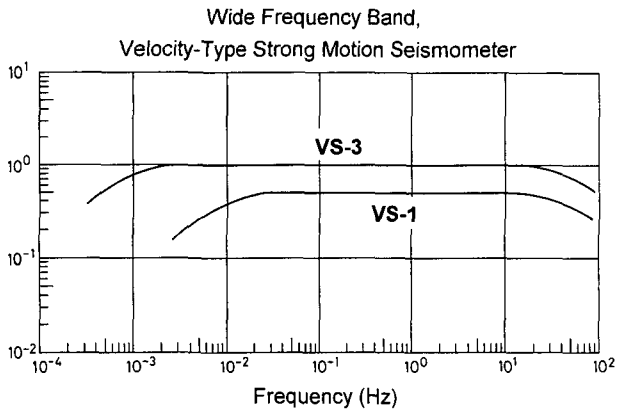


Fig. 6. Frequency characteristics of the velocity-type strong motion seismometers, VS-1 and VS-3 (Muramatu, 1995).

Table 1. Stations used in this study.

| Station | Instrument | 10/4 event | | 10/9 event | | Site condition |
|---|---|---|---|---|---|---|
| | | $\Delta$, km | Az. | $\Delta$, km | Az. | |
| KRK | VS-3 | 268 | 262 | 275 | 257 | Hill zone |
| TIS | VS-1 | 270 | 262 | 277 | 257 | Lowland<br>Alluvial thickness~100 m |
| OUV | VS-3 | 369 | 263 | 375 | 259 | Central part of the Tokachi basin<br>Thickness of sedimentary layer~600 m |
| MYR | VS-3 | 377 | 253 | 387 | 249 | Rock site |

$\Delta$=epicentral distance, Az.=epicenter to station azimuth in degree.

to our strong motion data. In this study, we assume a point source with a parabolic ramp source time function to roughly estimate the source parameters. A troublesome problem is the complex crustal structure from trench to island arc (Iwasaki et al., 1989) through which seismic waves propagate. However, ray paths from the hypocenters to our observation sites are nearly in parallel with the trench axis (Fig. 5(a)). We assume a simple flat layer crustal structure (Table 2), as a first approximation, modified from the island arc side structure of the Kurile continental slope model by Iwasaki. et al. (1989). The sea water is omitted.

We calculate synthetic seismograms based on the mechanisms shown in Fig. 5(a), (strike, dip, slip)=(49°, 75°, 125°) for the 10/4 event, (strike, dip, slip)=(33°,

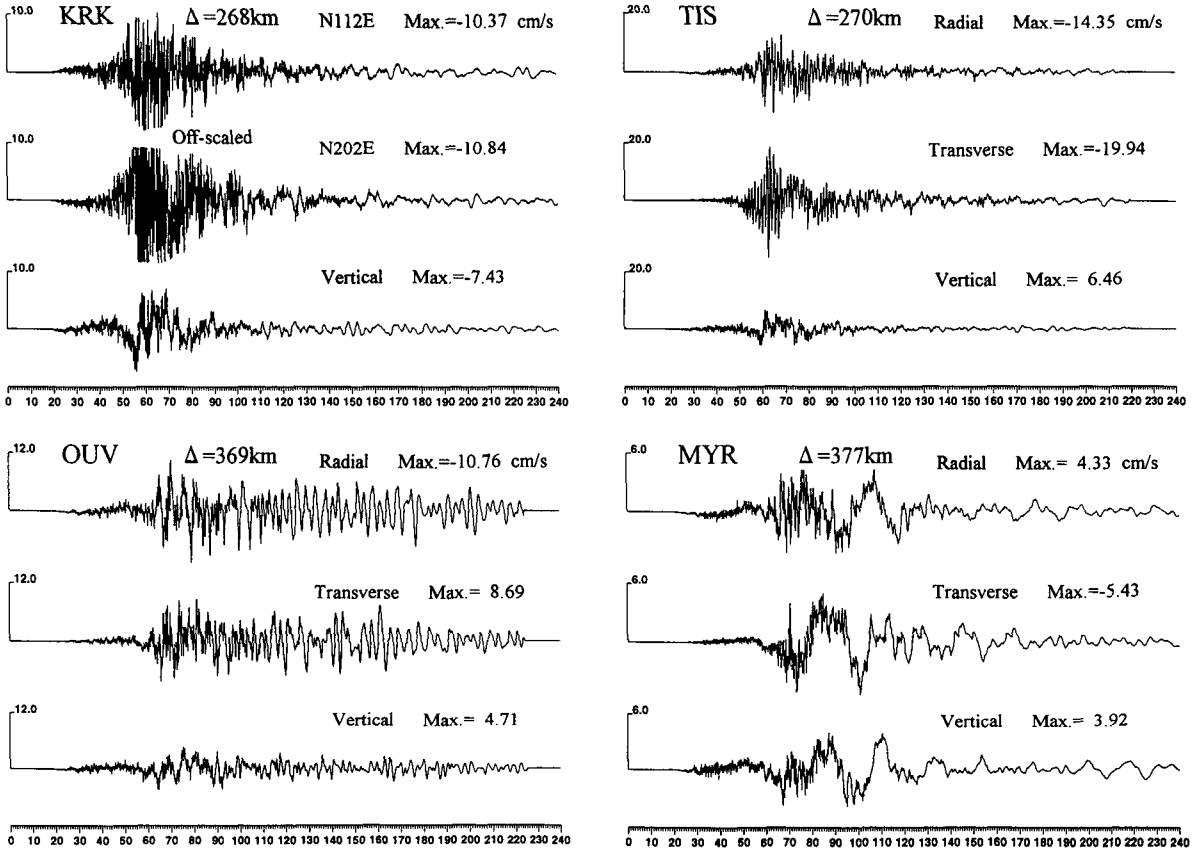


Fig. 7. Observed velocity seismograms at KRK, TIS, OUV and MYR during the main shock. Note that the horizontal components at KRK are off-scaled.

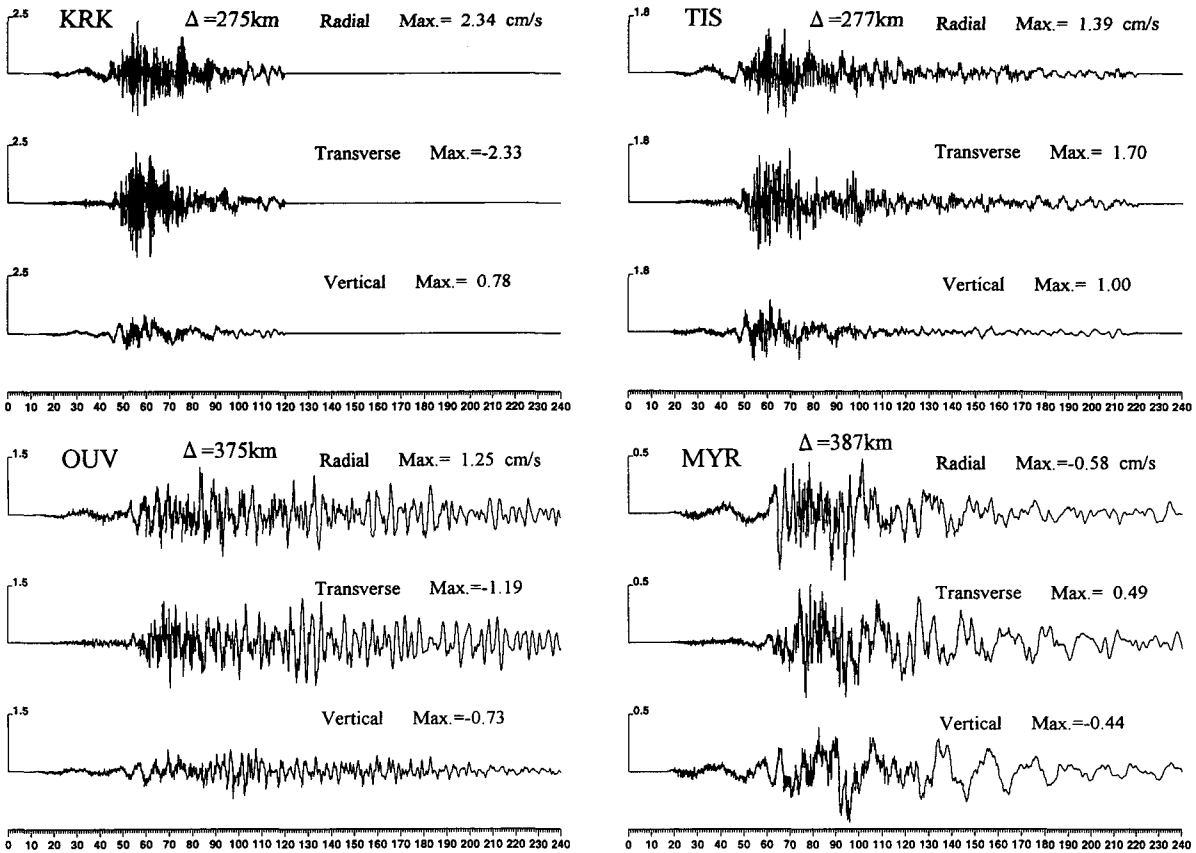


Fig. 8. Observed velocity seismograms at KRK, TIS, OUV and MYR during the largest aftershock.

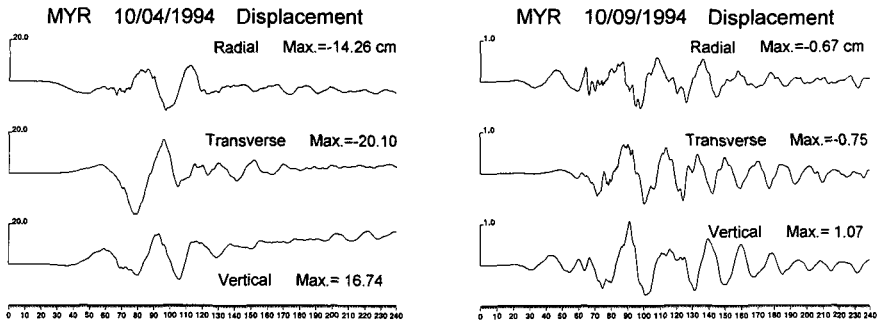


Fig. 9. An example of the displacement seismograms at MYR during the main (left) and the largest aftershock (right).

Table 2. Crustal structure assumed.

| P-vave velocity km/s | S-wave velocity km/s | Density g/cm$^3$ | Thickness km |
|---|---|---|---|
| 2.0 | 1.2 | 2.2 | 2.5 |
| 4.0 | 2.3 | 2.4 | 2.5 |
| 5.7 | 3.3 | 2.7 | 15.0 |
| 6.7 | 3.9 | 2.9 | 10.0 |
| 8.0 | 4.6 | 3.3 | 50.0 |
| 8.2 | 4.7 | 3.4 | — |

72°, 85°) for the 10/9 event; and assumptions mentioned above. The synthetic seismograms calculated by changing the focal depth ($H$) and the rise time ($T$) of the parabolic ramp function (source process time) are compared with the observed ones to estimate the reasonable source parameters. Figure 10 shows an example of the comparison at MYR between the observed seismograms and the synthetic ones calculated for various focal depths. For the 10/4 event, the synthetic waveforms of the transverse component do not so vary with focal depths, but those of the radial component strongly vary with focal depths. Considering the waveform similarity between the observed and synthetic seismograms for both components, we may conclude that this event has a focal depth of about 60 km. For the 10/9 event, the excitation strength of surface waves in the synthetic seismograms strongly vary with focal depths. The waveform comparison of the transverse component indicates a focal depth of about 25 km, but the comparison of the radial component indicates the more deeper depth. In this case we cannot have a harmonious estimation of the focal

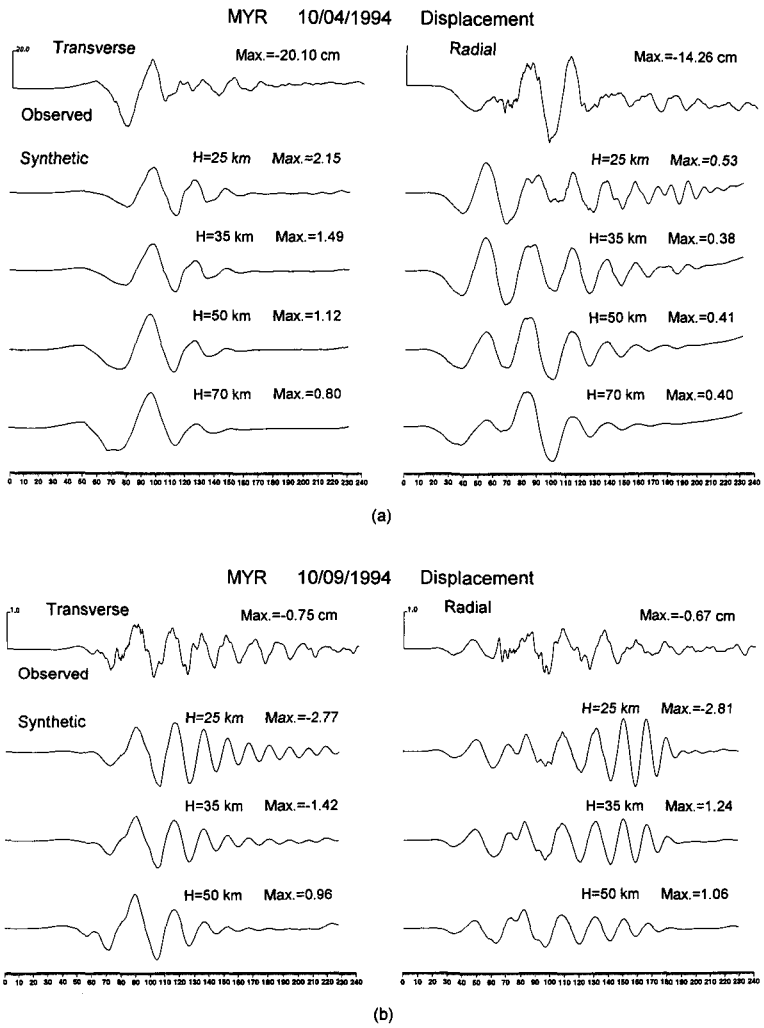


Fig. 10. (a) Comparison between the observed seismograms and the synthetic ones calculated for $M_0=10^{20}$Nm, T=30s and various focal depths at MYR for the main shock. (b) Comparison between the observed seismograms and the synthetic ones calculated for $M_0=10^{20}$Nm, T=15s and various focal depths at MYR for the largest aftershock.

depth from both components. However, comparing the waveforms for the first 150 seconds duration for both components, we may conclude that the focal depth is about 35 km.

We use mainly the transverse components to estimate source parameters.

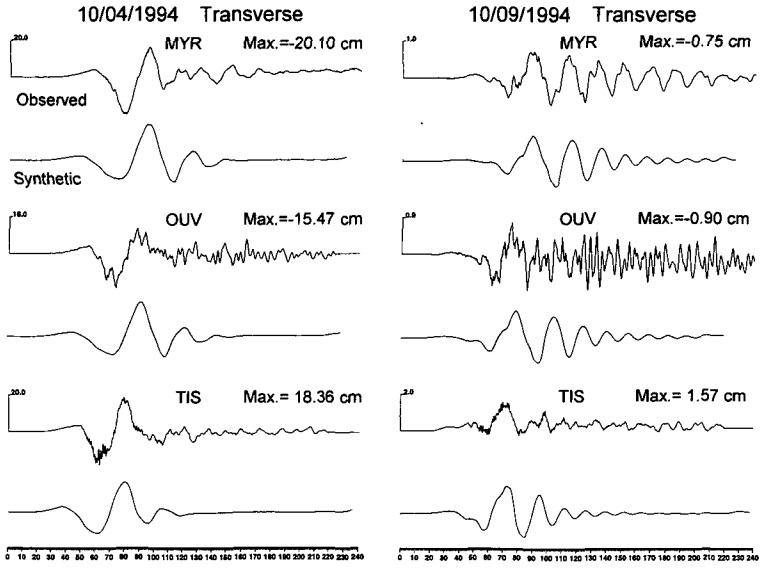


Fig. 11. Comparison between the observed and synthetic seismograms (transverse component) for the main shock (left) and the largest aftershock (right) at MYR, OUV and TIS. The synthetic seismograms are calculated for the estimated source parameters shown in Table 3.

Our final results are : (depth, $H$, source process time, $T$, seismic moment, $M_0$)= (60 km, 30s, $2.9\times10^{21}$Nm) for the 10/4 event and ($H$, $T$, $M_0$)=(35 km, 15 s, $8.5\times10^{19}$Nm) for the 10/9 event. Figure 11 shows a comparison between the observed and synthetic seismograms calculated for above parameters. An agreement is fairly good in spite of the simple calculation. In Table 3, we compare the source parameters of the 10/4 and 10/9 events estimated by various authors.

Table 3. Source parameters obtained by various authors.

| Event | Seismic moment $M_0$, Nm | Source process time $T$, s | Focal depth $H$, km | Peferences |
|---|---|---|---|---|
| 10/4 | $2.6\times10^{21}$ | 42 | 56 | Kikuchi and Kanamori (1995) |
| | 2.7 | 44* | ~50 | Tanioka et al. (1995) |
| | 3.0 | 25** | 68.2 | Dziewonski et al. (1995) |
| | 2.9 | 30 | ~60 | This study |
| 10/9 | $9.4\times10^{19}$ | 10.8** | 33.2 | Dziewonski et al. (1995) |
| | 8.5 | 15 | ~35 | This study |

*=roughly estimated from their moment tensor rate functions, **=half duration.

Our estimates are nearly the same as those obtained by other studies.

The important points are: 1) the 10/4 main shock with a distinct mechanism has the large centroid depth, while the 10/9 aftershock with a typical subduction mechanism has the considerably shallow depth near the plate boundary; 2) moment release density ($M_0/T$) for the 10/4 event is extremely higher than that for the 10/9 event. This indicates the high stress drop of the 10/4 event as pointed out by Kikuchi and Kanamori (1995).

## 4. Intermediate-Period Seismic waves

In order to extract more complex source process, we analyze velocity seismograms in which intermediate-period seismic waves predominate. The horizontal velocity seismograms are strongly affected by the site response (see Figs. 7 and 8) and are not useful to directly extract the source process informations. On the other hand, the vertical components are not severely affected by the site response as demonstrated by Campillo et al. (1989) and Sanchez-Sesma et al. (1993). Here we analyze the vertical velocity seismograms to extract the source process informations.

In the P-wave portion on the vertical velocity seismograms, interesting

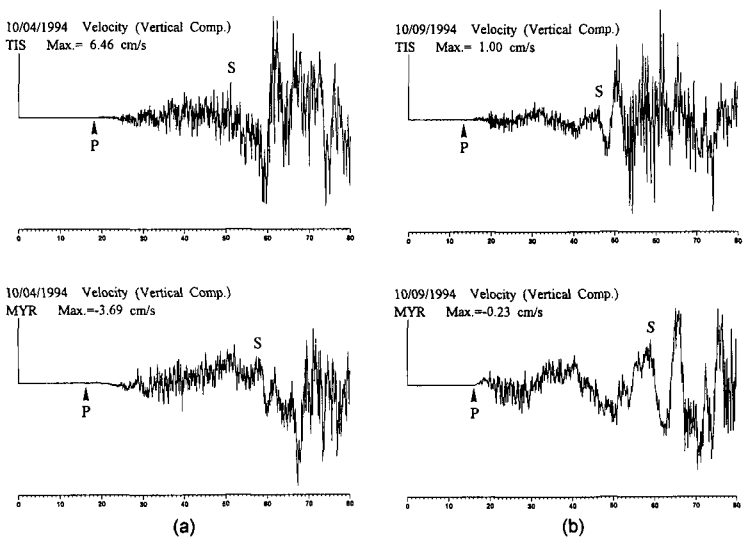


Fig. 12. An example of the observed vertical velocity seismograms. (a) The main shock, and (b) the largest aftershock. P indicates the first P-wave arrival and S, approximate S-wave arrival.

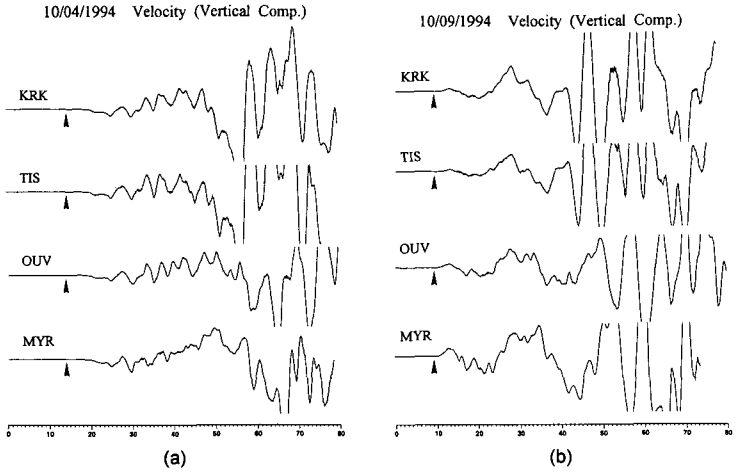


Fig. 13. High-cut filtered vertical velocity seismograms at KRK, TIS, OUV and MYR. (a) The main shock, and (b) the largest aftershock. Triangles indicate the first P-wave arrivals.

seismic waves with a period of several seconds are observed during the 10/4 event as shown in Fig. 12(a). We make high-cut filtered seismograms to clearly see these seismic waves (Fig. 13(a)). At 4 sites they have a similar wave shape ; several ripples appear about 10 seconds after the initial small, smooth phases, superposed with a long-period undulation, that is, the near-field term. Especially, the coherent ripples are observed at KRK, TIS and OUV ; these stations have approximately the same direction from the epicenter. Since the 10/4 event has the source process time of about 30s as obtained in the previous section, signals in the first 30s duration may be direct P waves from the seismic source. The original and the high-cut filtered vertical velocity seismograms for the 10/9 event are also shown in Figs. 12(b) and 13(b). On these seismograms, we do not see the clear, coherent ripples in the first 15s duration, the source process time of this event. This fact indicates that the strong ripples observed during the 10/4 event is not due to a path effect, but due to a source effect. One of the unique points of the 10/4 event source process is the generation of the several seconds period ripples.

Kikuchi and Kanamori (1995) inverted 32 body wave records to determine the rupture pattern of the 10/4 event in terms of a series of subevents. They found 6 subevents during the 42s source process time. The observed ripples on the vertical velocity seismograms for the 10/4 event may correspond to seismic signals due to the series of subevents. More detailed discussions about the

ripples are given in the later section.

Umeda (1990) analyzed the first parts of the vertical seismograms from several earthquakes and pointed out that two kinds of conspicuous phases could be found in the seismograms. One is the low-frequency, low-amplitude initial phase ($P_1$) and the other is the high-frequency, high-amplitude, second phase ($P_2$); $P_1$ and $P_2$ correspond to the rupture initiation and the generation of the bright spot, a small spot characterized by the production of high accelerations, respectively. In Figs. 12(a) and 13(a), we can see the initial small, smooth phases during about 10 s before the strong ripple appearance for the 10/4 event. These phases may correspond to the rupture initiation phases as pointed out by Umeda (1990). As discussed in the later section, the initial small, smooth phases follow the high frequency acceleration radiation (Fig. 17). Umeda (1990) also found that the time intervals between $P_1$ and $P_2$ phases increase in proportion to the earthquake magnitudes. The duration of the initial small, smooth phases for the 10/4 event ($M_{JMA}$ 8.1) almost satisfies the relationship between ($P_1$-$P_2$) times and earthquake magnitudes found by Umeda (1990). For the 10/9 event ($M_{JMA}$ 7.0), the initial phases have a duration of 2-3s, which also match the ($P_1$-$P_2$) times vs. magnitudes relationship by Umeda (1990).

## 5. Short-Period Seismic Waves

Finally we study a short-period seismic wave radiation problem in the frequency domain. Figure 14 shows S-wave acceleration spectra at MYR, OUV and TIS for the 10/4 and 10/9 events obtained by differentiating the

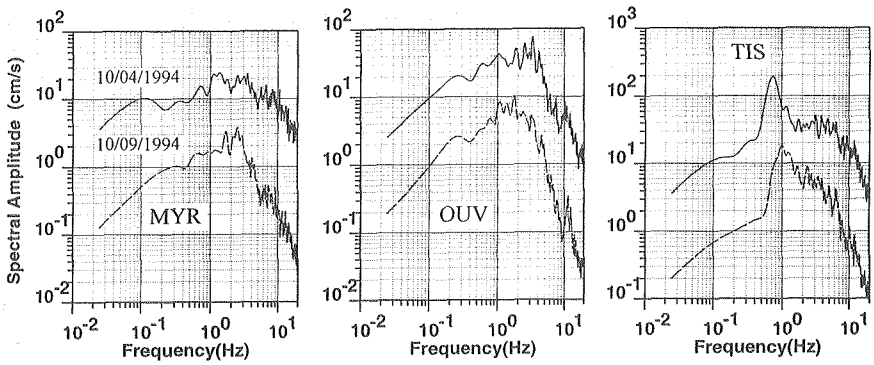


Fig. 14. S-wave acceleration spectra (transverse components) at MYR, OUV and TIS for the main shock (solid curves) and the largest aftershock (dashed curves).

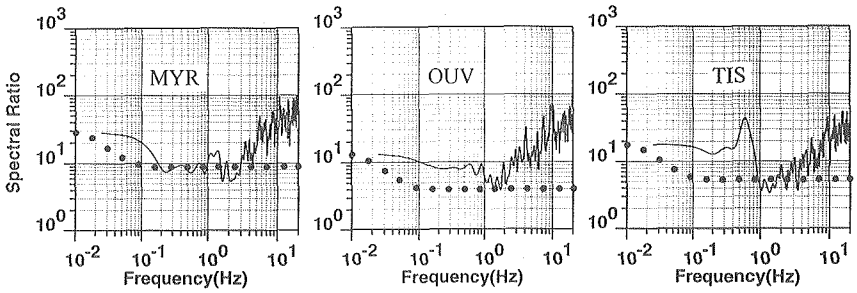


Fig. 15. S-wave spectral ratios (transverse components) of the main shock to the largest aftershock at MYR, OUV and TIS. Dotted curves are the reference curves based on the $\omega^{-2}$ source model (see text).

velocity spectra. These are obtained for 40s window of the transverse S-wave portion. The spectral shapes are different between the 10/4 event and the 10/9 event; especially at high frequencies the amplitude decay for the 10/9 event is greater than that for the 10/4 event. The spectral shapes also differ from site to site, which reflect the different site response as mentioned in the section 2. However, the spectral ratios of the 10/4 event to the 10/9 event have common features at these sites as shown in Fig. 15: at low frequencies ($f<0.05$ Hz) the ratios have a nearly flat level; at frequencies from 0.05 to 2 Hz, the ratios considerably decrease with frequency except TIS; and at high frequencies ($f>$ 2 Hz) the ratios conversely increase.

In order to interpret these features, we shall use reference curves based on the $\omega^{-2}$ source model (Singh et al., 1990). For $\omega^{-2}$ source model, observed acceleration spectrum can be written as

$$A(f)=CGM_0(2\pi f)^2 f_0^2 Q(f)/(f^2+f_0^2), \tag{1}$$

where $A(f)$=acceleration spectrum, $C$= source radiation effect, $G$=geometrical spreading effect, $M_0$=seismic moment, $f_0$=corner frequency and $Q(f)$= attenuation effect. The acceleration spectral ratio of event $i$ with respect to event $j$ is given by

$$A_i(f)/A_j(f)=[C_iG_iM_{0i}f_{0i}^2(f^2+f_{0j}^2)]/[C_jG_jM_{0j}f_{0j}^2(f^2+f_{0i}^2)], \tag{2}$$

$$=[C_iG_iM_{0i}]/[C_jG_jM_{0j}] \quad \text{for } f\ll f_{0i},\ f_{0j} \tag{3}$$

$$=[C_iG_iM_{0i}]/[C_jG_jM_{0j}]\cdot[f_{0i}^2/f_{0j}^2] \quad \text{for } f\gg f_{0i},\ f_{0j} \tag{4}$$

Here we assume $Q_i(f)\sim Q_j(f)$ for the present case. This may be a reasonable assumption because the 10/4 and 10/9 events have approximately the same epicenter as shown in Fig. 5(a). Predicted spectral ratio reference curves for

the 10/4 and 10/9 events are shown in Fig. 15. We can use directly the observed ratio level at low frequencies for equation (3). This is an advantage of our wide frequency band records. In computing $f_0$ in equations (2) and (4), we use $f_0=2/\pi T$ (source process time).

The reference curves roughly fit the observed spectral ratios at frequencies from 0.02 to 2 Hz except TIS ; the observed spectral ratio at TIS has a peak at about 0.6 Hz. At high frequencies ($f>2$ Hz), all the observed spectral ratios are greater than the reference curves. Especially, at frequencies of 10 to 20 Hz, the observed spectral ratios are about 10 times greater than the reference curves. Although the validity of the $\omega^{-2}$ source model for large and great earthquakes at high frequencies is uncertain, this indicates anomalously strong radiation of short-period (about 0.1s) seismic waves during the 10/4 event. Aftershock area of the 10/4 event (see Fig. 1) shows the rupture propagation in the south-west direction. Since our observation sites are located in nearly the same direction of the rupture propagation, a part of the anomalously strong radiation of short-period seismic waves may be attributed to a directivity effect (e.g., Campillo, 1983). The above interpretation explains the extremely large felt area (Fig. 2) and observed anomalously high peak horizontal accelerations (Fig. 3) during the 10/4 event.

At TIS, the amplitude spectrum for the 10/9 event has a peak at about 1 Hz, but it has a peak at about 0.7 Hz for the 10/4 event (Fig. 14). The observed spectral ratio peak at about 0.6 Hz at TIS is evidently due to this peak shift. The peak ground velocity at TIS is 20 cm/s during the 10/4 event, which is about 10 times larger than that (1.7 cm/s) during the 10/9 event. The observed spectral peak shift may be attributed to nonlinear soil response due to strong ground shaking (e.g., Iai et al., 1995 ; Aguirre and Irikura, 1995 ; Higashi and Sasatani, 1996).

## 6. Discussions and Conclusions

In Fig. 2, we show the extremely large felt area for the 1994 Hokkaido Toho-Oki earthquake (the 10/4 event) by comparing the felt area for the 1969 Kurile Islands earthquake. It is interesting to compare seismic records from these events which were obtained by a common instrument. At the time of the 1969 event occurrence, we had no wide frequency band instrument used in this study. However, we can compare records obtained by the JMA strong motion (displacement) seismograph ; the natural period, damping constant, and static magnification are 5-6 s, 0.5-0.6 and 1, respectively. Figure 16 shows the strong

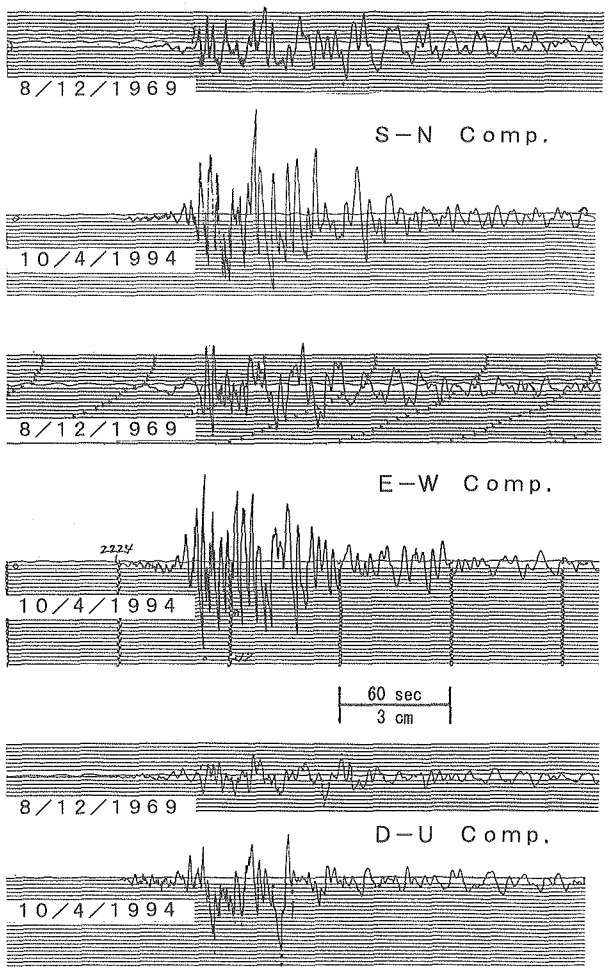


Fig. 16. Comparison between the JMA strong motion records at HOO during the 1969 Kurile Islands earthquake and the 1994 Hokkaido Toho-Oki earthquake.

motion records from the 1969 and 1994 events obtained at HOO (near our MYR station). The maximum amplitude for the 1994 event is about three times larger than that for the 1969 event. The short-period seismic waves are relatively rich for the 1994 event. These facts explain that the seismic intensity at HOO is 4 for the 1969 event, but 5 for the 1994 event (see Fig. 2). Although the more detailed comparison is difficult because of their analog records, this figure depicts much stronger seismic energy radiation during the 1994 event. We can point out an another interesting feature. The surface wave amplitudes

compared with S-wave amplitudes for the 1994 event are much smaller than those for the 1969 event. This qualitatively indicates the relatively deeper focal depth for the 1994 event, and supports our focal depth estimation.

The 1969 Kurile Islands earthquake is a typical plate boundary earthquake (Abe, 1973) and the 1994 Hokkaido Toho-Oki earthquake (the 10/4 event) is a lithospheric earthquake as shown in the previous section. The seismic moments of these events are nearly the same (Fig. 2), but the intermediate- to short-period seismic wave radiation is evidently different as shown in Fig. 16. This indicates the different source spectra between the plate boundary and the lithospheric earthquakes; the lithospheric earthquake more strongly radiates short-period seismic waves. The spectral ratios of the 10/4 event to the 10/9 event in Fig. 15 show an another example of the different source spectra between the plate boundary and the lithospheric earthquakes.

We have shown two unique points of the source process of the 1994 Hokkaido Toho-Oki earthquake (the 10/4 event); the ripples with a period of several seconds in the vertical component P-wave portion, and anomalously strong radiation of short-period seismic waves indicated by S-wave spectra in the frequency domain. It is very important to directly examine the relation between the ripples and short period seismic wave radiation in the time domain. In Fig. 17, we compare the vertical component accelerograms, in which short-period seismic waves predominate, and the low-pass filtered, vertical component velocity seismograms (same as Fig. 13) for the 10/4 and 10/9 events. The accelerograms are obtained by differentiating the velocity records. The acceleration level for the initial small, smooth phases on the velocity seismogram is extremely low, but the acceleration level grows up in proportion to the ripple amplitude during the 10/4 event. This indicates that the ripples observed during the 10/4 event are intimately related to the short-period seismic wave radiation. On the other hand, for the 10/9 event, the acceleration level decreases after the first 15s duration (the source process time of this event), and the apparent ripples observed at the later times do not grow up the acceleration level. This indicates that the apparent ripples observed during the 10/9 event are not a source effect but a path effect. We conclude from this examination that the ripples and the strong radiation of short-period seismic waves observed during the 10/4 event have a cause-and-effect relationship.

The theoretical consideration by Das and Aki (1977) showed that the presence of barriers on the fault plane offered a physical basis for the idea of multiple shocks and also for the cause of ripples in the seismogram. They also demonstrated that the barrier failure produces strong short-period radiation.

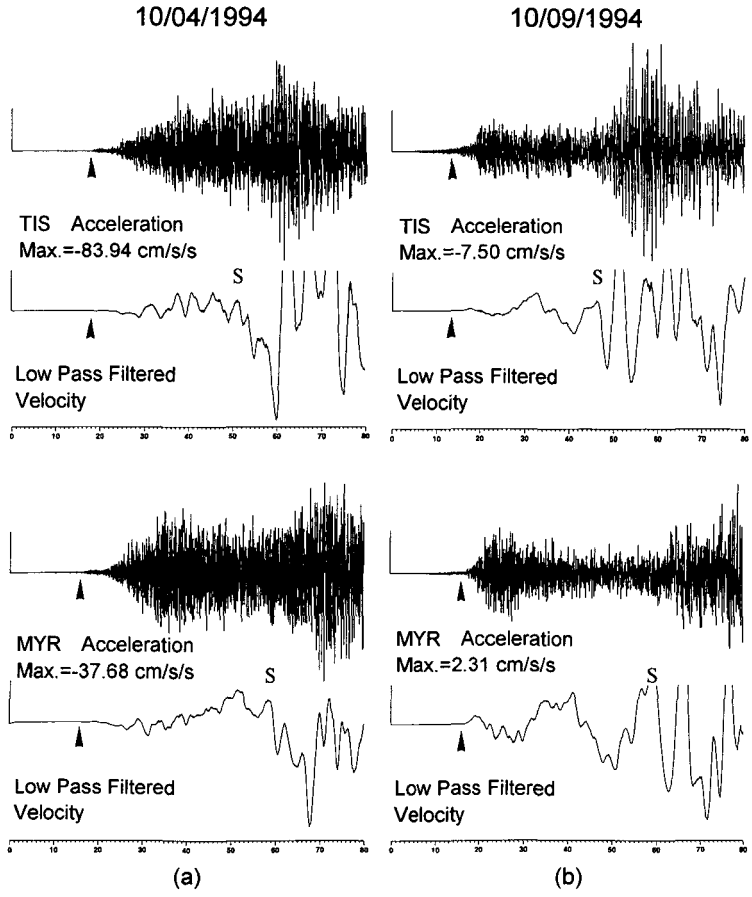


Fig. 17. Relationship between the vertical accelerograms and the low pass filtered, vertical velocity seismograms in the P-wave portion at TIS and MYR. (a) The main shock, and (b) the largest aftershock. Triangles indicate the first P-wave arrivals and S, approximate S-wave arrival.

Our findings of the ripples and anomalously strong radiation of short-period seismic waves during the 10/4 event may be explained by this fault model with barriers. In fact, Kikuchi and Kanamori (1995) found a series of 6 subevents during the 42s source process time for the 10/4 event, which may correspond to the several ripples observed during this event. Campillo et al. (1989) proposed a somewhat different model to explain the ripples in the seismogram. They explained the 3s period ripples observed at Caleta de Campos during the 1985 Michoacan, Mexico earthquake by a self-similar crack model with a series of

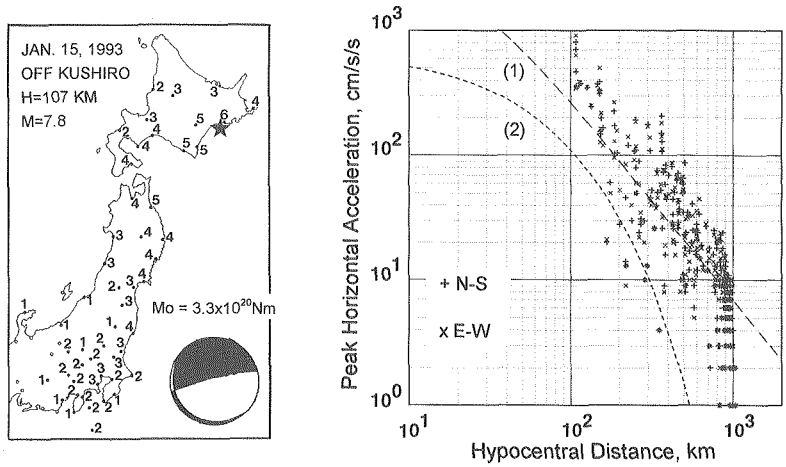


Fig. 18. (a) Distribution of seismic intensities (JMA scale) for the 1993 Kushiro-Oki earthquake. Also shown is the focal mechanism by Takeo et al. (1993). (b) Relationship between peak horizontal accelerations and hypocentral distances for the 1993 Kushiro-Oki earthquake. For curves (1) and (2), see the caption of Fig. 3.

changes of the rupture front velocity. The theoretical studies show that changes of the rupture velocity will result in emission of short-period seismic waves (e.g., Campillo, 1983). It is difficult to know which of the models is reasonable to explain the observed ripples and strong radiation of short-period seismic waves during the 10/4 event based on only our data. In any case, the existence of the ripples indicates the complex source process which radiates strong short-period seismic waves.

A destructive lithospheric earthquake ($M_{JMA}$ 7.8; $H=107$ km) occurred beneath Kushiro city on January 15, 1993. This event ruptured the lithosphere along the nearly horizontal fault plane (Kasahara et al., 1993). The felt area is considerably large (Fig. 18(a)) and the observed peak horizontal accelerations are extremely larger than those expected from the empirical attenuation relations (Fig. 18(b)). The wide band strong motion records during the 1993 Kushiro-Oki earthquake were obtained at MYR by the VS-3 instrument. We examine the records using the same methods as applied to the 1994 Hokkaido Toho-Oki earthquake records. In Fig. 19(a), we show the vertical component accelerogram; the low-pass filtered, vertical component velocity seismogram; and the original vertical component velocity seismogram at MYR during this event.

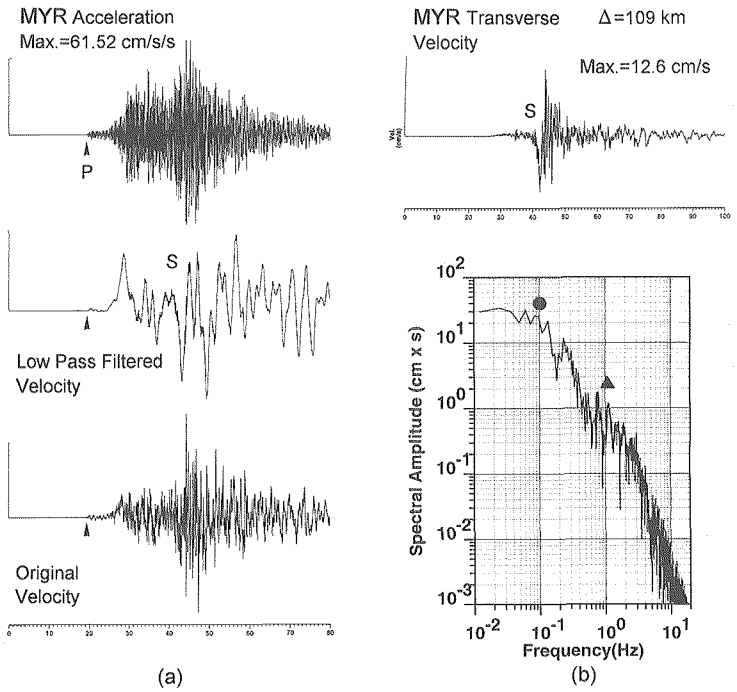


Fig. 19. (a) Relationship between the vertical accelerogram (upper) and the low pass filtered, vertical velocity seismogram (middle) in the P-wave portion at MYR for the 1993 Kushiro-Oki earthquake. The lower trace is the original velocity record. (b) S-wave (transverse component) displacement spectrum at MYR for the 1993 Kushiro-Oki earthquake. A solid circle and a solid triangle represent the first and the second corner frequencies (Mahdavian and Sasatani, 1996). The upper trace is the transverse velocity seismogram.

The accelerogram and the low-pass filtered velocity seismogram are obtained from the original velocity seismogram. A few distinctive ripples appear about 7s after the first small, smooth phases (the rupture initiation phases) and acceleration level grows up in proportion to the ripple amplitude. Since the main source process time of this event is about 10s (Takeo et al., 1993), the observed ripples are not due to a path effect but due to a source effect. Furthermore, Mahdavian and Sasatani (1996) pointed out that the S-wave spectrum from this event has two corner frequencies (Fig. 19(b)), indicating anomalously strong radiation of short-period seismic waves. These observations during the 1993 Kushiro-Oki earthquake show very similar features as observed during the 1994 Hokkaido Toho-Oki earthquake; these may be specific features of large lithospheric earthquakes. The strong motion seismo-

logical implication of above features is that the large lithospheric earthquakes such as the 1993 Kushiro-Oki and the 1994 Hokkaido Toho-Oki earthquakes show a departure from the simple scaling law, especially at high frequencies.

## Acknowledgments

I thank Dr. M. Furumura, Dr. S. Saito and Mr. H. Nagumo of Hokkaido University and Professor T. Koyanagi of Obihiro University of Agriculture and Veterinary Medicine for their cooperation with strong motion observations. I also thank the staffs of HOO observatory who provide me with the strong motion data used in this study.

## References

Abe, K., 1973. Tsunami and mechanism of great earthquakes. Phys. Earth Planet. Inter., **7**, 143-153.

Aguirre, J. and K. Irikura, 1995. Preliminary analysis of non-linear site effects at Port Island vertical array station during the 1995 Hyogoken-Nambu earthquake. J. Natural Disast. Sci., **16**, 49-58.

Architectural Institute of Japan, 1996. Report on the damage investigation of the 1994 Hokkaido-Toho-Oki earthquake and the 1994 Sanriku-Haruka-Oki earthquake. pp. 506 (in Japanese).

Campillo, M., 1983. Numerical evaluation of near-field, high-frequency radiation from quasi dynamic circular faults. Bull. Seism. Soc. Am., **73**, 723-734.

Campillo, M., J.C. Gariel, K. Aki, and F.J. Sanchez-Sesma, 1989. Destructive strong ground motion in Mexico city: Source, path, and site effects during great 1985 Michoacan earthquakes. Bull. Seism. Soc. Am., **79**, 1718-1735.

Das, S. and K. Aki., 1977. Fault plane with barriers: A versatile earthquake model. J. Geophys. Res., **82**, 5658-5670.

Dziewonski, A.M., G. Ekstrom, and P.M. Salganik, 1995. Centroid-moment tensor solutions for October-December 1994. Phys. Earth Planet. Inter., **91**, 187-201.

Fukao, Y. and M. Furumoto, 1979. Stress drops, wave spectra and recurrence intervals of great earthquakes-Implication of the Etorofu earthquake of 1958 November 6. Geophys. J. R. Astro. Soc., **57**, 23-40.

Fukushima, Y. and T. Tanaka, 1990. A new attenuation relation for peak horizontal acceleration of strong earthquake ground motion in Japan. Bull. Seism. Soc. Am., **80**, 757-783.

Furumura, M. and T. Sasatani, 1996. Secondarily generated surface waves in the Tokachi basin, Hokkaido, Japan. J. Phys. Earth., **44**, 115-132.

Higashi, S. and T. Sasatani, 1996. Nonlinear ground response in Kushiro during the 1994 Hokkaido Toho-Oki earthquake. Programme and Abstracts, Seism. Soc. Japan, 1996, No. 2, C04.

Iai, S., T. Morita, T. Kameoka, Y. Matsunaga and K. Abiko, 1995. Response of a dense sand deposit during 1993 Kushiro-Oki earthquake. Soils and Foundations, **35**, 115-131.

Iwasaki, T., H. Shiobara, A. Nishizawa, T. Kanazawa, K. Suyehiro, N. Hirata, T. Urabe and H. Shimamura, 1989. A detailed subduction structure in the Kurile trench deduced

from oceanic seismographic refraction studies. Tectonophys., **165**, 315-336.
Kanai, K., K. Hirano, S. Yoshizawa and T. Asada, 1966. Observation of strong earthquake motions in Matsushiro area. Part 1, (Empirical formulae of strong earthquake motions). Bull. Earthq. Res. Inst., **44**, 1269-1296.
Kasahara, M., S. Kodaira, and Y. Motoya, 1993. Aftershock sequence of the large intermediate-depth Kushiro-oki earthquake of January 15, 1993 and 16 years' seismicity around Hokkaido before quake. Report on the disaster by the 1993 Kushiro-oki earthquake, Hokkaido University, Sapporo, pp. 27-33 (in Japanese).
Kikuchi, M. and H. Kanamori (1995). The Shikotan earthquake of October 4, 1994 : Lithospheric earthquake. Geophys. Res. Lett., **22**, 1025-1028.
Mahdavian, A. and T. Sasatani, 1996. S-wave spectra from strong motion seismograms: Source parameters and site response. J. Fac. Sci. Hokkaido Univ., Ser. VII (Geophys.), **10**, 1-19.
Matsushima, T., 1990. Studies on determination of deep geological structures using long-period microtremors. Ph.D. thesis, Hokkaido University, pp. 133 (in Japanese with English abstract).
Muramatu, I. 1995. Development of a broadband velocity type strong motion seismometers and its recording range. Zisin, **48**, 247-256 (in Japanese).
Sanchez-Sesma, F.J., L.E. Perez-Rocha and E. Reinoso, 1993. Ground motion in Mexico city during the April 25, 1989, Guerrero earthquake. Tectonophys., **218**, 127-140.
Sasatani, T., 1966. Site effects in Kushiro during the 1993 Kushiro-Oki and 1994 Hokkaido Toho-Oki earthquakes. Special Theme Section on Effect of surface geology on strong ground motion, Proc. of 11th World Conference on Earthquake Engineering, 2029.
Sekiguchi, H., K. Irikura, T. Iwata, Y. Kakehi, and M. Hoshiba, 1996. Minute locating fault planes and source process of the 1995 Hyogo-ken Nanbu (Kobe), Japan, earthquake from the waveform inversion of strong ground motion. J. Phys. Earth, in press.
Singh, S.K., A. Mori, E. Mena, F. Kruger and R. Kind, 1990. Evidence for anomalous body wave radiation between 0.3 and 0.7 Hz from the 1985 September 19 Michoacan, Mexico earthquake. Geophys. J. Int., **101**, 37-48.
Takemura, M., 1987. Attenuation of seismic waves in the Earth and attenuation curves. The 15th Symposium on ground vibrations, Architectural Institute of Japan, pp. 33-46 (in Japanese).
Takeo, M., S. Ide, and Y. Yoshida, 1993. The 1993 Kushiro-Oki, Japan, earthquake: A high stress-drop event in a subducting slab. Geophys. Res. Lett., **20**, 2607-2610.
Tanioka, Y., L. Ruff and K. Satake, 1995. The great Kurile earthquake of October 4, 1994 tore the slab. Geophys. Res. Lett., **22**, 1661-1664.
Umeda, Y., 1990. High-amplitude seismic waves radiated from the bright spot of an earthquake. Tectonophys., **175**, 81-92.
Utsu, T., 1972. Large earthquakes near Hokkaido and the expectancy of the occurrence of a large earthquake off Nemuro. Rep. Coord. Comm. Earthq. Prediction, **7**, 7-13 (in Japanese).
Wald, D.J., T.H. Heaton, and K.W. Hudnut, 1996. The slip history of the 1994 Northridge, California, earthquake determined from strong-motion, teleseismic, GPS, and Leveling data. Bull, Seism, Soc, Am., **86**, S49-S70.